J. Fluid Mech. (1982), *vol.* 115, *pp.* 475–492
Printed in Great Britain

Collisions between two solitary waves. Part 2. A numerical study

By RIDA M. MIRIE† AND C. H. SU

Division of Applied Mathematics,
Brown University, Providence, RI 02912, U.S.A.

(Received 28 August 1980)

Collisions between two solitary waves are investigated using a numerical scheme. The phase shifts and maximum amplitude of a collision are checked with a corresponding perturbation calculation and compared with the available experiments. We found a wave train trailing behind each of the emerging solitary waves from a head-on collision. The properties of the wave train are in agreement with those of the perturbation solution. After the collision, the solitary waves recover almost all of their original amplitude for the length of time in our calculation. However, the difference (less than 2 % of their original value) persists and accounts for the energy residing in the wave train.

1. Introduction

Recently Su & Mirie (1980, hereinafter referred to as paper 1) considered head-on collisions of two surface solitary waves in an inviscid, incompressible, homogeneous fluid by a perturbation method up to the third order of approximation. They found that the solitary waves emerging from a collision, in addition to having experienced changes of their phases, were trailed by a dispersive wave train.

In this paper we shall present a numerical calculation of the collisions of two solitary waves. Our emphasis will be on the verification of the generation of the secondary waves as predicted in paper 1. We shall use a set of equations derived by Su & Gardner (1969) for the following reasons.

(i) These equations give the same secondary-wave system as in paper 1 up to the third order of approximation. This will be amplified in § 2, where the results of a perturbation calculation of these equations will be given. A comparison with the corresponding result in paper 1 will also be presented.

(ii) These equations contain lower-order partial derivatives than the ones used in paper 1. The reduction of the order of derivatives facilitates the numerical scheme to be presented in § 3.

(iii) These equations have an exact solitary-wave solution.

Since the equations derived in Su & Gardner are obtained by discarding the fifth- and higher-order derivative terms of the exact equation, they have the same accuracy as Boussinesq's equation in shallow water. The phase shift and the maximum amplitude in our numerical result are correct up to that order only.

In § 2 we shall list the results of perturbation calculations of the equations derived

* Present address: Department of Math. Sciences, University of Petroleum and Minerals, Dhahran, Saudi Arabia.

in Su & Gardner following the method in paper 1. A comparison of these results to those in paper 1 will also be given here. In § 3 we present our numerical scheme. The numerical results are given in § 4, where we study the reflection (or head-on collision of two identical solitary waves) of a solitary wave from a vertical wall. We also study the head-on collision of solitary waves of different amplitudes. The appearance of a wave train behind each emerging solitary wave, as predicted in paper 1, is confirmed by these numerical experiments.

Maxworthy (1976) has indicated the existence of a secondary wave in his experiments on the reflection of a solitary wave by a vertical wall. However, the surface profile he gave is too crude to make a quantitative comparison. There are also a number of theoretical works on perturbed solitons based mainly on the K–dV equation. A perturbation method based on the inverse-scattering technique was given by Karpman (1979). A variational perturbation method was given by Bondeson, Lisak & Anderson (1979). Numerical integration of a perturbed K–dV equation was given by Fernandez *et al.* (1978). All of these works considered the evolution of a soliton under some perturbation, and all indicated the presence of a wave train. Abdulleov, Bogolubsky & Makhankov (1976), and later Bona, Pritchard & Scott (1980) integrated numerically a variant of the K–dV equation (replacing u_{xxx} by u_{xxt}) and found a dispersive wave train after an overtaking collision of two solitary waves.

We have carried out one calculation for an overtaking collision between two solitary waves. Our results on phase shifts and the time history of interaction agree with the theoretical solution of the Korteweg–de Vries equation (see the last paragraph of § 4). The amplitude of the wave train in this calculation is, however, of the same size as the numerical error. Further study is needed to ascertain the existence of any dispersive wave train in an overtaking collision, using an equation that is a better approximation to the exact water-wave equation than the Korteweg–de Vries equation.

2. The equations of motion

We consider an inviscid, incompressible, homogeneous fluid layer on a horizontal bed. Using the long-wave assumption, Su & Gardner (1969) obtained

$$h_t + [hu]_x = 0, \tag{1}$$

$$[hu]_t + [hu^2 + \tfrac{1}{2}gh^2 - \tfrac{1}{3}h^3(u_{xt} + uu_{xx} - u_x^2)]_x = 0, \tag{2}$$

where h and u are the height of the fluid surface and the average horizontal velocity respectively, and g is the acceleration due to gravity. Equation (1) represents the continuity equation, while (2) represents the momentum-conservation law. These equations can also be derived from the exact equations in paper 1 by discarding all derivatives of order five and greater.

Two more conservation laws representing the energy and the Bernoulli relation can be derived from (1) and (2), namely

$$[hu^2 + gh^2 + \tfrac{1}{3}h^3u_x^2]_t + [hu(u^2 + 2gh) - \tfrac{2}{3}h^3u(u_{xt} + uu_{xx} - \tfrac{3}{2}u_x^2)]_x = 0, \tag{3}$$

$$[u - \tfrac{1}{3}hh_xu_x]_t + [\tfrac{1}{2}u^2 + gh - \tfrac{1}{3}h^2(u_{xt} + uu_{xx} - \tfrac{1}{2}u_x^2) - \tfrac{1}{3}hh_xuu_x]_x = 0. \tag{4}$$

Equations (1) and (2), or any two out of these four equations, admit one solitary-wave solution:

$$h = h_0\left[1 + A\,\mathrm{sech}^2\frac{k}{2h_0}(x - ct + x_0)\right], \quad u = c\left[1 - \frac{1}{h}\right], \tag{5}$$

where

$$\frac{c^2}{gh_0} = 1+A, \quad k = \left(\frac{3A}{1+A}\right)^{\frac{1}{2}}.$$

A, c, k stand for the wave amplitude, wave speed and wavenumber respectively; h_0 is the undisturbed depth of the fluid, and x_0 is a phase constant.

Using the perturbation methods in paper 1, we obtain the following solution of (1) and (2) for the weak interaction (head-on collision) of two solitary waves (for details see Mirie 1980). The free-surface elevation is given by

$$h = h_0[1+AF+BG+\tfrac{1}{2}ABFG+\tfrac{11}{8}ABFG(AF+BG)-\tfrac{9}{8}ABFG(A+B)], \tag{6}$$

and the average horizontal velocity by

$$\begin{aligned}\frac{u}{(gh_0)^{\frac{1}{2}}} = {} & [AF+A^2(-F^2+\tfrac{1}{2}F)+A^3(F^3-\tfrac{1}{2}F^2-\tfrac{1}{8}F)-BG-B^2(-G^2+\tfrac{1}{2}G) \\ & -B^3(G^3-\tfrac{1}{2}G^2-\tfrac{1}{8}G)+\tfrac{3}{8}ABFG(BG-AF)+\tfrac{1}{8}ABFG(A-B)], \end{aligned} \tag{7}$$

where

$$F = \operatorname{sech}^2\tfrac{1}{2}\xi, \quad G = \operatorname{sech}^2\tfrac{1}{2}\eta, \tag{8}$$

$$\xi = \frac{k}{h_0}(x-c_Rt+\theta(\xi,\eta)), \tag{9a}$$

$$\eta = \frac{l}{h_0}(x+c_Lt+\psi(\xi,\eta)), \tag{9b}$$

$$k^2 = \frac{3A}{1+A}, \quad l^2 = \frac{3B}{1+B}, \quad \frac{c_R^2}{gh_0} = 1+A, \quad \frac{c_L^2}{gh_0} = 1+B. \tag{10}$$

A and B represent the wave amplitudes of the right- and left-going waves respectively. The phase functions θ and ψ are given as follows:

$$\theta(\xi,\eta) = \tfrac{1}{4}h_0(\tfrac{1}{3}B)^{\frac{1}{2}}\left\{\int_{-\infty}^{\eta}[1+\tfrac{4}{3}BG-\tfrac{13}{4}A-\tfrac{1}{4}B]G\,d\eta+9AF\int_{-\infty}^{\eta}G\,d\eta\right\}, \tag{11}$$

$$\psi(\xi,\eta) = \tfrac{1}{4}h_0(\tfrac{1}{3}A)^{\frac{1}{2}}\left\{\int_{+\infty}^{\xi}[1+\tfrac{4}{3}AF-\tfrac{13}{4}B-\tfrac{1}{4}A]F\,d\xi+9BG\int_{+\infty}^{\xi}F\,d\xi\right\}. \tag{12}$$

As η (ξ) tends to positive (negative) infinity, the quantities in (11) and (12) represent the phase shifts of the right- and left-going solitary waves respectively. The first integral in (11) represents a simple phase shift, i.e. it is constant in the limit $\eta \to \infty$; the second integral (which is identical with a corresponding term in equation (53) of paper 1) is the source for the production of the secondary wave train. As $\eta \to \infty$ this term gives a ξ-dependent phase shift that represents an asymmetrical distortion of the wave profile. We have demonstrated that this asymmetrical distortion evolves into two parts, one consisting of a uniform phase shift and the other a dispersive wave train as given by equation (76) in paper 1. The asymptotic behaviour of the wave train long after collision, as obtained by the method of steepest descent, was also given. The wave train trails behind the solitary wave that gave birth to it. It consists of an exponential leading edge followed by a series of oscillatory waves with decreasing wavelength and amplitude. For later comparison with the numerical results, we further simplify the expression for the wavelets (equation (77) in paper 1)

under the assumption of a large separation between the solitary wave and the wave train. The deviation of the water surface is then given by

$$\zeta = 8\epsilon_R^3 \left(\frac{\pi}{6\tau}\right)^{\frac{1}{2}} \frac{K_0^{\frac{3}{2}}(1+K_0^2)}{\sinh \pi K_0} \cos(\tau K_0^3 - \tfrac{1}{4}\pi + \phi), \tag{13}$$

where

$$K_0^2 = \frac{1}{3}\left(\frac{x}{x_0} - 1\right), \quad \phi = \arccos \frac{2K_0}{1+K_0^2},$$

x is the horizontal distance from the centre of the solitary wave, and x_0 is related to τ by $2\epsilon_R^{\frac{1}{2}} k x_0 = \tau$ or defined as the value of x which makes $K_0 = 0$. It turns out that x_0 is very close to the point where the exponential and the oscillatory parts of the wave train meet (a point of inflection).

We will be particularly interested in the variation of amplitude and wavelength in the wave train. To study the latter we consider the zeros of (13). It is easy to verify that any three adjacent zeros x_1, x_2, x_3 will satisfy the following simple relationship:

$$(x_1 - x_0)^{\frac{3}{2}} + (x_3 - x_0)^{\frac{3}{2}} = 2(x_2 - x_0)^{\frac{3}{2}}. \tag{14}$$

The positions of the peaks in the wave train also satisfy this relation.

The total (uniform) phase shifts of the right- and left-going waves are given respectively by

$$\Delta\theta = h_0(\tfrac{1}{3}B)^{\frac{1}{2}}(1 + \tfrac{1}{4}B + \tfrac{3}{4}A), \tag{15a}$$

$$\Delta\psi = -h_0(\tfrac{1}{3}A)^{\frac{1}{2}}(1 + \tfrac{1}{4}A + \tfrac{3}{4}B). \tag{16a}$$

The maximum amplitude (run-up) during the collision is obtained from (6) by setting $F = G = 1$ in $h/h_0 - 1$, i.e.

$$\text{maximum run-up} = A + B + \tfrac{1}{2}AB + \tfrac{1}{4}(AB^2 + BA^2). \tag{17a}$$

The corresponding formulas from paper 1 are

$$(\Delta\theta)_1 = h_0(\tfrac{1}{3}\epsilon_L)^{\frac{1}{2}}(1 + \tfrac{1}{8}\epsilon_L + \tfrac{3}{4}\epsilon_R), \tag{15b}$$

$$(\Delta\psi)_1 = -h_0(\tfrac{1}{3}\epsilon_R)^{\frac{1}{2}}(1 + \tfrac{1}{8}\epsilon_R + \tfrac{3}{4}\epsilon_L), \tag{16b}$$

$$(\text{maximum run-up})_1 = \epsilon_R + \epsilon_L + \tfrac{1}{2}\epsilon_R\epsilon_L + \tfrac{3}{8}\epsilon_R\epsilon_L(\epsilon_R + \epsilon_L). \tag{17b}$$

The quantities ϵ_R and ϵ_L in (15b)–(17b) represent the amplitude of the right- and left-going waves and are equivalent to A and B in (15a)–(17a). The differences between these two sets of results numbered from 15 to 17 with sub-designation a and b, represent the errors in the truncated equations to be used in our numerical calculation. We shall check the numerical results of phase shifts and maximum amplitude with the first set of these equations (designated with a). The characteristics of the wave train of the truncated equation are, however, exactly the same as those of the exact equation.

3. The numerical method

We now rewrite the equations of motion (1) and (4) in terms of non-dimensional variables defined by

$$\bar{u} = \frac{u}{(gh_0)^{\frac{1}{2}}}, \quad \bar{h} = \frac{h}{h_0}, \quad \bar{x} = \frac{x}{h_0}, \quad \bar{t} = t\left(\frac{g}{h_0}\right)^{\frac{1}{2}}, \quad \bar{c} = \frac{c}{(gh_0)^{\frac{1}{2}}},$$

We also group all terms involving time derivatives in (4) into a new variable. We obtain, after deleting the 'bar', the following equations:

$$h_t + [hu]_x = 0, \tag{18}$$

$$v_t + [uv - \tfrac{1}{2}u^2 + h - \tfrac{1}{3}h^2 u_x^2]_x = 0, \tag{19}$$

where

$$v = u - \frac{1}{3h}(h^3 u_x)_x. \tag{20}$$

Equations (18) and (19) serve to advance h and v in time. At each time step we use (20) to determine a new u. The process is then repeated for a new time step and this allows us to advance h and u (or v) for any finite number of time steps. The scheme avoids dealing with mixed derivatives in (4). The original initial-value problem in u is thus replaced by a simpler initial-value problem coupled with a boundary-value problem.

The co-ordinates x and t are discretized by a grid spacing Δx and a time step Δt. This gives the grid points $(i\Delta x, j\Delta t)$, where i and j are integers. The solutions are obtained step-by-step in time. First a provisional value h_i^{*j+1} is obtained from (18) by the following finite-difference scheme:

$$\frac{h_i^{*j+1} - h_i^j}{\Delta t} + \tfrac{1}{2}(h_i^{*j+1} + h_i^j)\left(\frac{u_{i+1}^j - u_{i-1}^j}{2\Delta x}\right) + u_i^j\left(\frac{h_{i+1}^{*j+1} - h_{i-1}^{*j+1} + h_{i+1}^j - h_{i-1}^j}{4\Delta x}\right) = 0. \tag{21}$$

Then a provisional value v_i^{*j+1} is obtained from (19) by

$$\begin{aligned}\frac{v_i^{*j+1} - v_i^j}{\Delta t} &+ \tfrac{1}{2}(v_i^{*j+1} + v_i^j)\left(\frac{u_{i+1}^j - u_{i-1}^j}{2\Delta x}\right) + u_i^j\left(\frac{v_{i+1}^{*j+1} - v_{i-1}^{*j+1} + v_{i+1}^j - v_{i-1}^j}{4\Delta x}\right)\\ &- u_i^j\left(\frac{u_{i+1}^j - u_{i-1}^j}{2\Delta x}\right) - \tfrac{1}{4}(h_i^{*j+1} + h_i^j)^2\left(\frac{u_{i+1}^j - u_{i-1}^j}{2\Delta x}\right)\left(\frac{u_{i+1}^j - 2u_i^j + u_{i-1}^j}{(\Delta x)^2}\right)\\ &+ \left(\frac{h_{i+1}^{*j+1} - h_{i-1}^{*j+1} + h_{i+1}^j - h_{i-1}^j}{4\Delta x}\right)\left[1 - \tfrac{1}{2}(h_i^{*j+1} + h_i^j)\left(\frac{u_{i+1}^j - u_{i-1}^j}{2\Delta x}\right)\right] = 0.\end{aligned} \tag{22}$$

Thirdly, at the new time step the horizontal velocity u is obtained from (20) by using the provisional values of h and v, i.e.

$$\begin{aligned}v_i^{*j+1} = u_i^{j+1} - h_i^{*j+1}&\left(\frac{h_{i+1}^{*j+1} - h_{i-1}^{*j+1}}{2\Delta x}\right)\left(\frac{u_{i+1}^{j+1} - u_{i-1}^{j+1}}{2\Delta x}\right)\\ &- \tfrac{1}{3}(h_i^{*j+1})^2\left(\frac{u_{i+1}^{j+1} - 2u_i^{j+1} + u_{i-1}^{j+1}}{(\Delta x)^2}\right).\end{aligned} \tag{23}$$

Lastly, we calculate the corrected values h_i^{j+1} and v_i^{j+1} from (21) and (22) by replacing u_i^j by $\frac{1}{2}(u_i^j + u_i^{j+1})$. The solution for $h_i^{*j+1}, v_i^{*j+1}, u_i^{j+1}, h_i^{j+1}, v_i^{j+1}$ involves solving a tri-diagonal system of equations for each variable at each time step.

The use of a provisional value was introduced by Peregrine (1966). He used $\xi = h - 1$ in the continuity equation and a linearized dispersion term u_{xxt} in the Bernoulli equation to calculate the development of an undular bore.

We also introduce the following tests of the numerical method. The system of

Conservation law	Formula	Simpson rule initial	Reflection: 1512 time steps, actual time = 75·6	Reflection: 2412 time steps, actual time = 165·6	Free motion: 783 time steps, actual time = 39·15
Mass	2·0000000	2.0000000	2.0001534	2·0001215	1·9997590
Energy	5·4379240	5·4379933	5·4376097	5·4337147	5·4372805
Momentum	2·4494897	2·4497724	2·4514732	2·4489286	2·4497032
Bernoulli	1·8197607	1·8199869	1·8188769	1·8179994	1·8200174

TABLE 1

equations under consideration, (1)–(4), provides four constants of motion. For a solitary-wave motion as given in (5), these four constants of motion are as follows:

$$\int_{-\infty}^{\infty} (h-1)\,dx = \frac{4A}{k}, \tag{24}$$

$$\int_{-\infty}^{\infty} hv\,dx = \int_{-\infty}^{\infty} hu\,dx = \frac{4AC}{k}, \tag{25}$$

$$\int_{-\infty}^{\infty} v\,dx = \int_{-\infty}^{\infty} u - \tfrac{1}{3}hh_x u_x\,dx = -\frac{4AC}{k} + \frac{8A^2}{3kC} + \frac{8C}{k}\left(\frac{A}{1+A}\right)^{\frac{1}{2}} \ln\left[A^{\frac{1}{2}} + (1+A)^{\frac{1}{2}}\right] \tag{26}$$

$$\int_{-\infty}^{\infty} (huv + h^2 - 1)\,dx = \int_{-\infty}^{\infty} (hu^2 + h^2 + \tfrac{1}{3}h^3u_x^2 - 1)\,dx$$

$$= \frac{8A}{k}(1+C^2) - \frac{8C^2}{k}\left(\frac{A}{1+A}\right)^{\frac{1}{2}} \ln\left[A^{\frac{1}{2}} + (1+A)^{\frac{1}{2}}\right]. \tag{27}$$

C is positive or negative depending on whether the wave is moving to the right or left. The above four constants of motion will be calculated by the Simpson rule to test the numerical method.

In a key test we let a solitary wave of amplitude 0·5 travel thrice its effective wavelength in a moving grid of 800 points with $\Delta x = 0{\cdot}1, \Delta t = 0{\cdot}05$. In table 1 we give the results of this calculation. We found that the differences in h, u, v from the corresponding exact values as given by (5) are no more than $3{\cdot}4 \times 10^{-3}$ at the end of integration. Such results could be improved if one used a larger, stationary range of integration.

The tests on the constancy of the four constants of motion will also be used on the numerical method for the interaction of two solitary waves.

4. Numerical results

(i) *Reflection of a solitary wave from a wall*

This is the same as the head-on collision of two identical solitary waves. The solitary wave was stationed away from the wall such that the initial value of $h-1$ at the wall was less than 0·00001. The boundary conditions at the wall are $u = 0, v = 0, h_x = 0$. At the other end of the range of integration we impose an exponential decay of h, u, v to their undisturbed values. We start with a solitary wave of amplitude 0·5 in a grid of 480 points with $\Delta x = 0{\cdot}1$ and $\Delta t = 0{\cdot}05$ as in figure 1, where we have also plotted

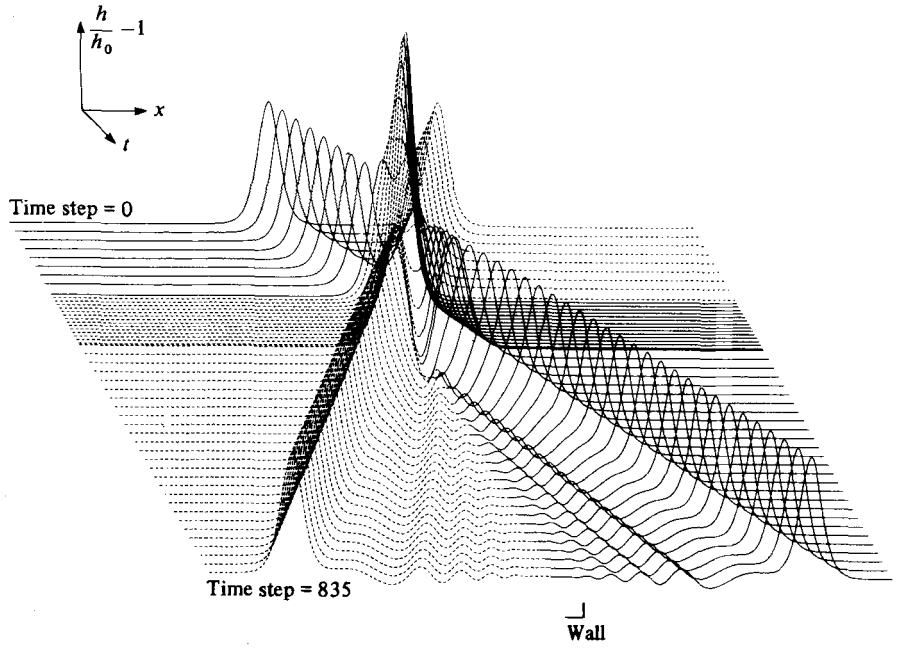

FIGURE 1. Surface elevation versus x and t of a solitary wave of amplitude 0·5 reflecting from a wall. The image profile is included.

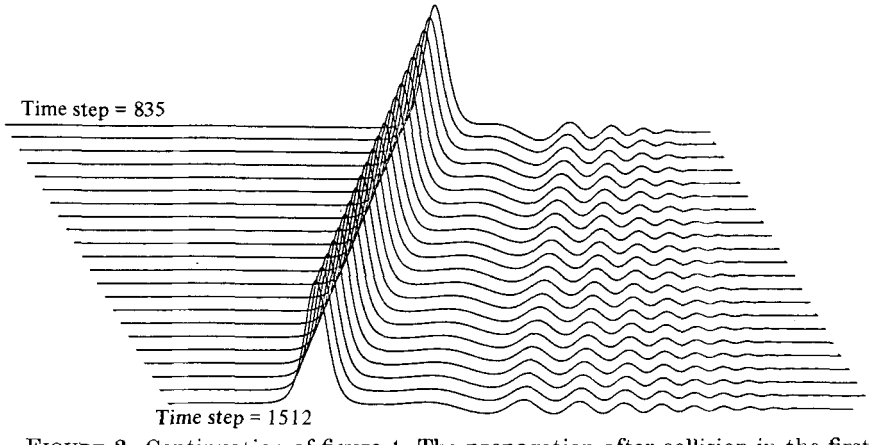

FIGURE 2. Continuation of figure 1. The propagation after collision in the first extension for time steps 835–1512, $\Delta t = 0{\cdot}05$.

the profile of the image solitary wave at different time steps. After the wave was reflected from the wall we twice extended the free end of the range so that the values of h, u, v there remained reasonably small. At time step 835 the number of grid points was enlarged to 960. Later, at time step 1512, the number of grid points was set to 2000 and Δt was set to 0·1. We carried the integration till time step 2412. The motion of the reflected wave in the first extension is plotted for various time steps in figure 2. In the second phase we plot the last profile with the initial profile (see figure 3). Our calculations confirm the existence of a dispersive secondary-wave system. The

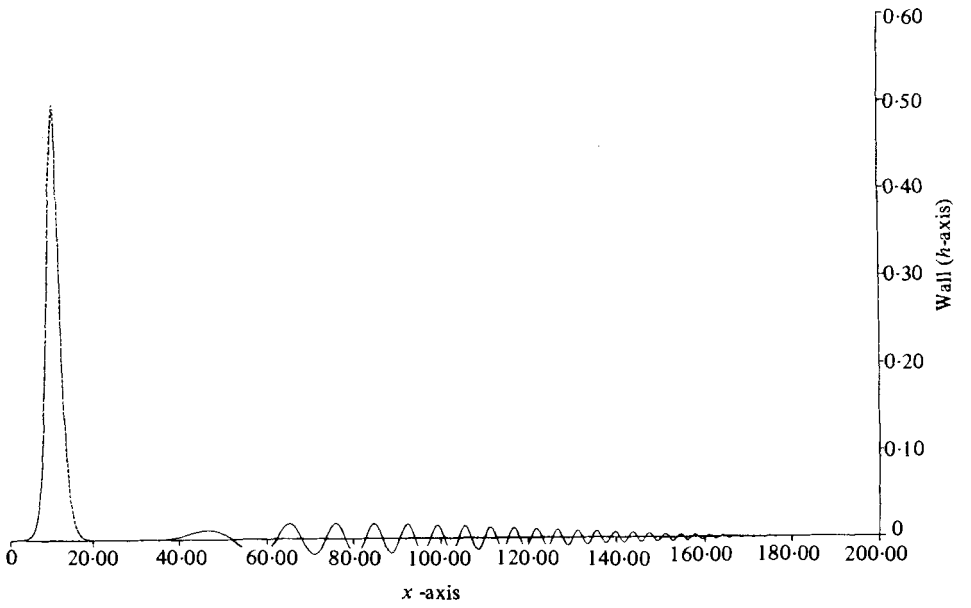

FIGURE 3. Comparison of surface elevation (solid line) at the time step 2412 with the initial solitary wave (dotted line) versus x. Actual time = 165·60; amplitude = 0·5.

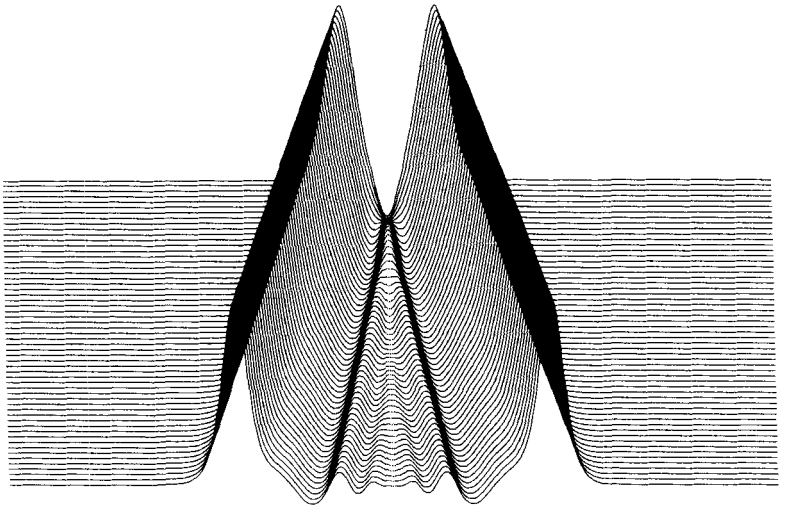

FIGURE 4. Birth of the wave train. Elevation versus x and t. The image profile is included.

amplitude and wavelength of these wave trains at any fixed time decrease as the distance from the main wave increases.

The reflected solitary wave in figure 3 has regained 98 % of its original amplitude. The energy deficit in this reflected solitary wave is, according to (27), 2 % of its original value. This deficit is made up by the amount of energy residing in the wave train. The numerical error in the constancy of total energy as indicated in table 1 is 0·077 % of the energy in the solitary wave before collision. We shall come back to this at the end of this subsection.

1512 time steps; actual time = 75·6

Numerical					
K^3 (zero)	K^3 (peak)	Amplitude (peak)	Equation (14) K^3 (zero)	Equation (14) K^3 (peak)	Equation (13) amplitude (peak)
0·0721	0·1573	0·0213	0·1138	0·1517	0·0246
0·2275	0·2824	0·0273	0·2039	0·2760	0·0249
0·3356	0·3947	0·0260	0·3407	0·3927	0·0247
0·4538	0·5031	0·0241	0·4464	0·5006	0·0243
0·5572	0·6065	0·0221	0·5572	0·6061	0·0238
0·6606	0·7092	0·0199	0·6563	0·7063	0·0234
0·7553	0·8061	0·0178	0·7574	0·8043	0·0229
0·8542	0·8994	0·0157	0·8484	0·8972	0·0224
0·9415	0·9882	0·0138	0·9469	0·9896	0·0220
1·0396	1·0798	0·0119	1·0310	1·0749	0·0216
1·1204	1·1615	0·0103	1·1235	1·1625	0·0212
1·2074	1·2453	0·0087	1·2041	1·2441	0·0208
1·2879	1·3266	0·0073	1·2887	1·3253	0·0204

2412 time steps; actual time = 165·6

Numerical					
K^3 (zero)	K^3 (peak)	Amplitude (peak)	Equation (14) K^3 (zero)	Equation (14) K^3 (peak)	Equation (13) amplitude (peak)
0·0318	0·0666	0·0167	0·0474	0·0633	0·0149
0·0948	0·1174	0·0174	0·0859	0·1160	0·0156
0·1399	0·1655	0·0179	0·1422	0·1643	0·0159
0·1897	0·2112	0·0177	0·1862	0·2109	0·0160
0·2324	0·2563	0·0176	0·2348	0·2556	0·0161
0·2800	0·3000	0·0171	0·2765	0·2995	0·0160
0·3205	0·3426	0·0168	0·3226	0·3424	0·0160
0·3652	0·3847	0·0163	0·3626	0·3843	0·0159
0·4046	0·4260	0·0158	0·4065	0·4261	0·0158
0·4478	0·4675	0·0153	0·4454	0·4668	0·0157
0·4862	0·5076	0·0147	0·4880	0·5069	0·0156
0·5281	0·5463	0·0141	0·5261	0·5468	0·0155
0·5660	0·5859	0·0135	0·5671	0·5856	0·0154
0·6060	0·6250	0·0129	0·6044	0·6240	0·0153
0·6428	0·6622	0·0123	0·6439	0·6625	0·0152
0·6817	0·7000	0·0117	0·6800	0·6997	0·0151
0·7171	0·7372	0·0112	0·7189	0·7368	0·0149
0·7560	0·7735	0·0106	0·7541	0·7730	0·0148
0·7911	0·8089	0·0099	0·7921	0·8092	0·0147
0·8283	0·8448	0·0095	0·8263	0·8443	0·0146
0·8615	0·8797	0·0089	0·8640	0·8800	0·0145
0·8997	0·9151	0·0084	0·8968	0·9146	0·0144
0·9322	0·9494	0·0079	0·9578	0·9496	0·0143

TABLE 2

We would like to point out in figure 1 the rapid falling of the water surface at the wall following its attainment of the maximum elevation there. The vertical velocity there reaches a value equal to half the linear wave speed $(gh_0)^{\frac{1}{2}}$. It seems very plausible that this downpour of water is the physical cause of the generation of the wave train as depicted in figure 4.

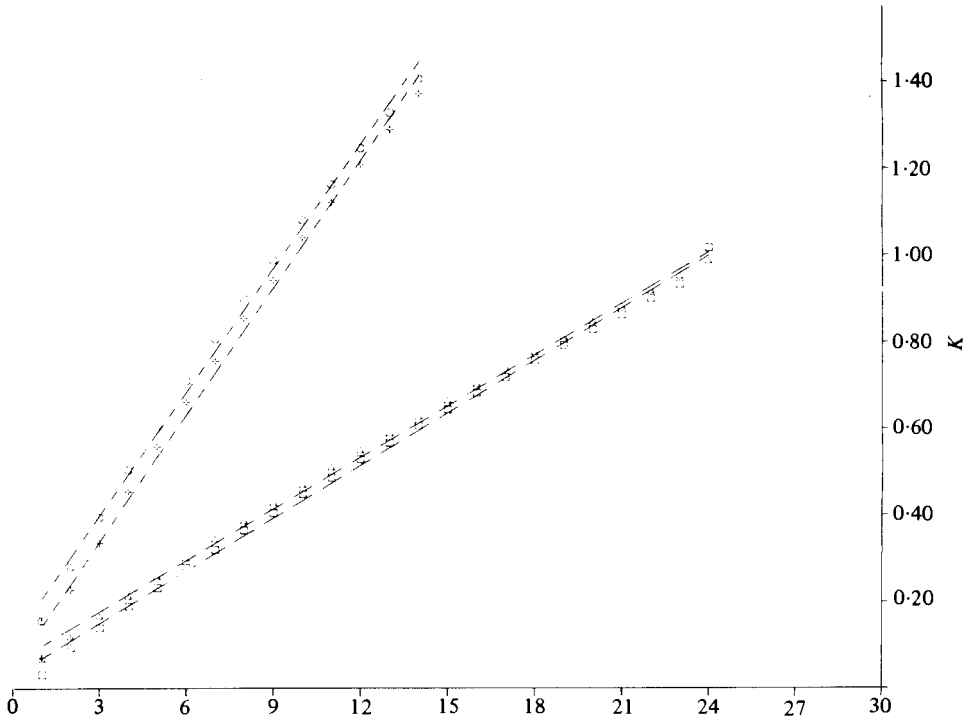

FIGURE 5. $K^3 = (3x_0)^{-\frac{3}{2}}(x-x_0)^{\frac{3}{2}}$ of extrema and zeros of wave train at time steps 1512, 2412 (○, × ; □, △) versus the number. The dashed lines are their respective least-square approximation by a straight line.

The decrease in the wavelength and amplitude in the wave train is clearly perceptible in figures 1 and 2. In table 2 we verify the wavelength variation as given by (14) for the time steps 1512 and 2412. Also given are the calculated positions of the extrema in the wave train and those given by (14). In figure 5, the value of $K_0^3 = (x/3x_0 - 1)^{\frac{3}{2}}$ at the extrema and zeros for time steps 1512 and 2412 is plotted versus the number of the extremum or zero, respectively. Also included is the linear least-square approximation of each.

The absolute values of the maxima and minima of the wave train at two time steps (1512, 2412) are plotted in figure 6. This shows the decrease in amplitude and dispersion of the wave train in time. In table 2, we list these values in the third column in order of increasing distance from the main wave. The corresponding values from the theoretical result as given by (13) are listed in the last column. Comparison of these two columns (third and sixth) shows that the agreement is good for those wavelets not too far from the main wave. The numerical calculation gives faster decay of the wave train as a function of distance from the main wave than that predicted by the perturbation analysis.

Four more cases of solitary waves of amplitude 0·31, 0·2; 0·1 and 0·05 with $\Delta x = 0{\cdot}1$, $\Delta t = 0{\cdot}05$ and grid length of 480 points were integrated. The phase shifts for each case are plotted in figure 7, along with the first-order solutions of Byatt-Smith (1971), Oikawa & Yajima (1973), and (15*a*, *b*). We have also plotted the experimental results of Maxworthy (1976). To the accuracy of our calculations the phase shift is amplitude dependent and lies 6–17 % above the corresponding theoretical predictions. This is

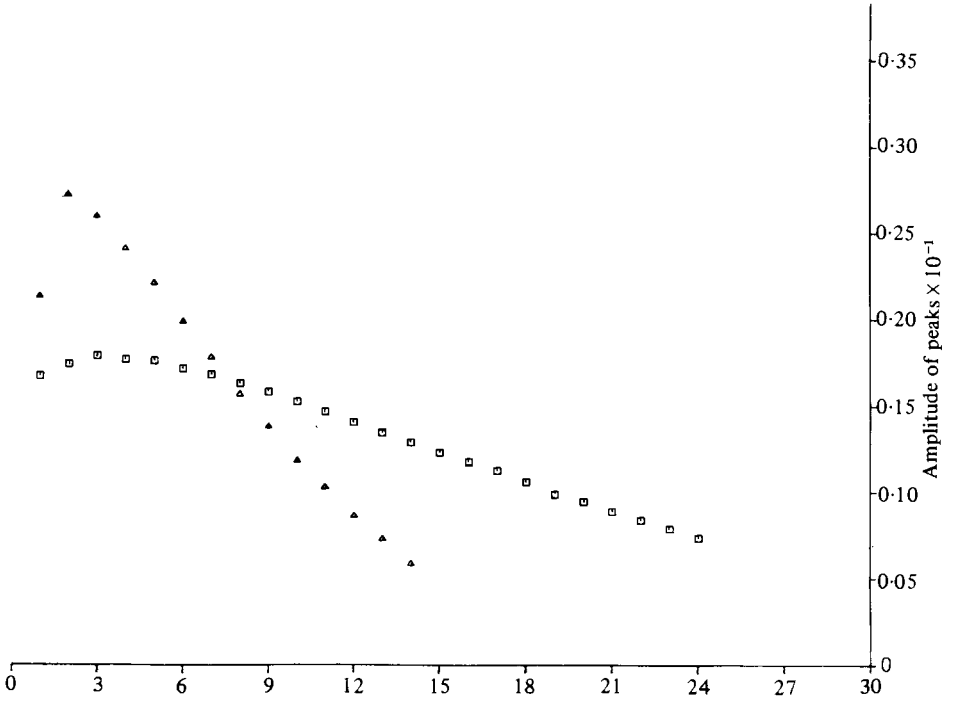

FIGURE 6. Amplitude of extrema of wave train at time steps 1512 (△), 2412 (□) versus extrema number.

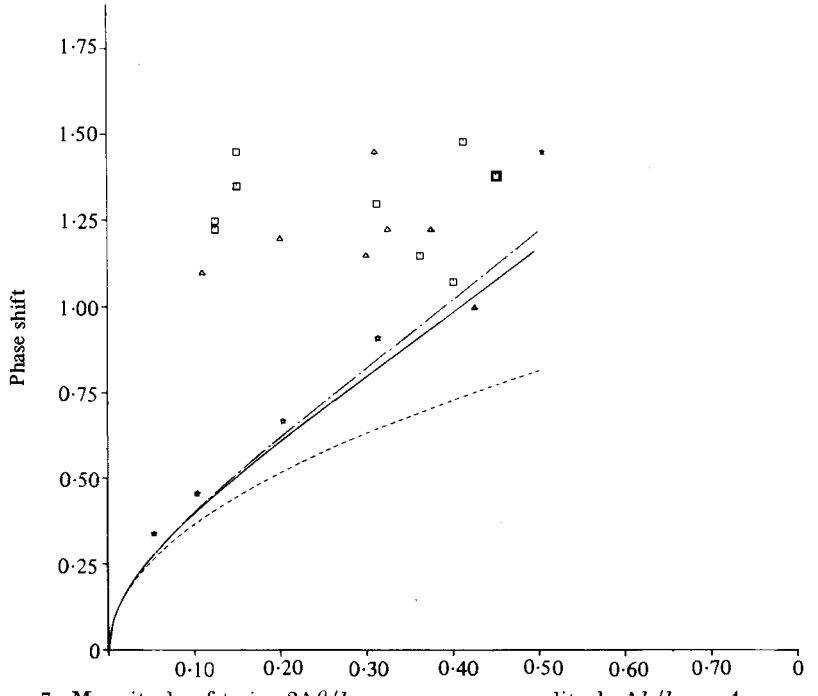

FIGURE 7. Magnitude of twice $2\Delta\theta/h_0$ versus wave amplitude $\Delta h/h_0 = A$. ——, (17*b*); — · —, (17*a*); ☆, numerical results; . . ., Oikawa & Yajima (1973) and implicit result from Byatt-Smith (1971); △, Maxworthy's (1976) wave–wave interaction; □, end-wall reflection.

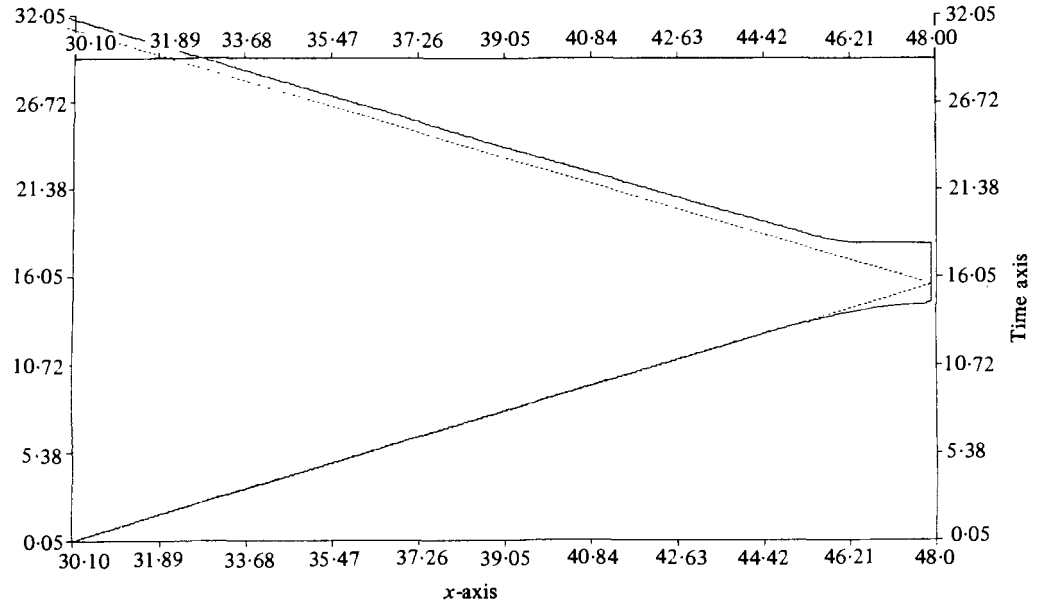

FIGURE 8. A typical example (amplitude = 0·31) of phase shift evaluation. ——, position of the highest level of water versus time; ..., trajectory of a non-interacting solitary wave. Amplitude = 0·31.

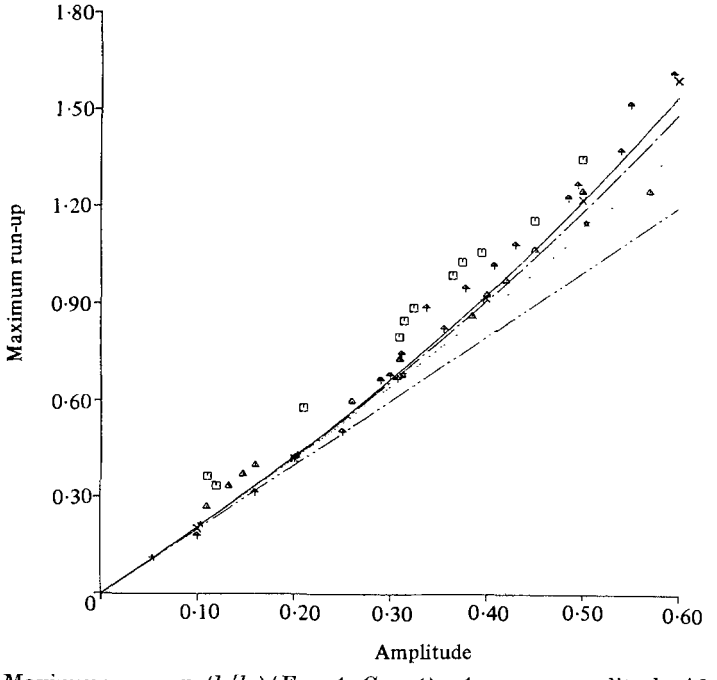

FIGURE 9. Maximum run-up $(h/h_0)(F = 1, G = 1) - 1$ versus amplitude $\Delta h/h_0 = A$. — · · —, first-order; ..., second-order; — · —, (17*a*); ——, (17*b*); *, numerical; ×, Chan & Street (1971) numerical; ⏃, Camfield & Street (1969) experimental; △, Maxworthy's (1976) end-wall reflection; □, wave–wave interaction.

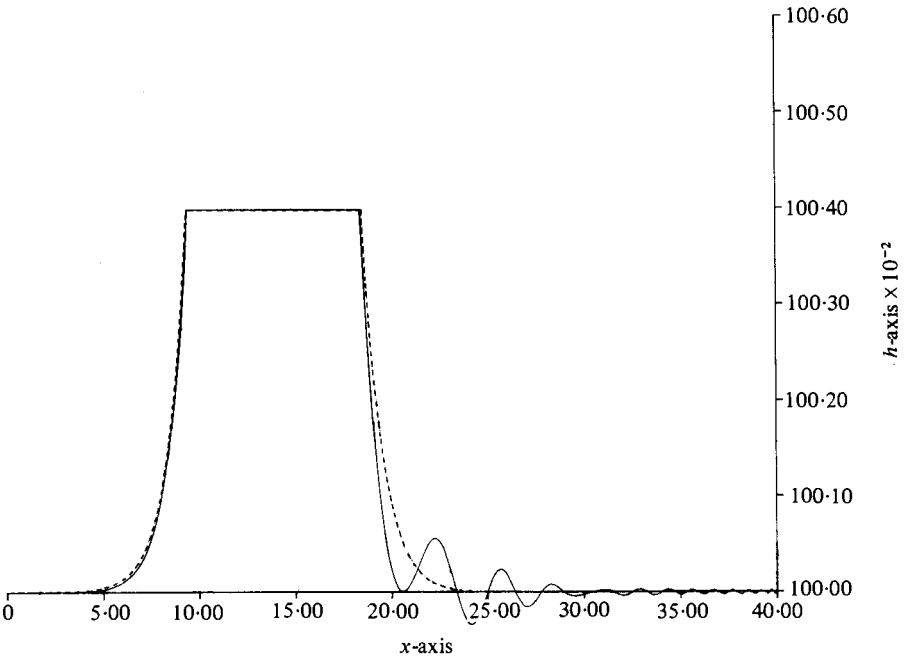

FIGURE 10. Comparison of 0·1 amplitude reflected solitary wave. Elevation (——) and initial profile (. . . .) versus u at time step = 3740. Actual time = 34·451; amplitude = 0·1.

because of the slightly smaller amplitude and thus smaller wave speeds of the reflected waves. A typical phase-shift calculation is given in figure 8 for the case of the amplitude equal to 0·31. The trajectory of the point of maximum amplitude of the solitary wave is plotted. The intercept on the time axis can be calculated by using (6). We obtained a value of $2{\cdot}85(h_0/g)^{\frac{1}{2}}$ by taking the first four terms while the numerical value is $2{\cdot}88(h_0/g)^{\frac{1}{2}}$.

The maximum run-up calculations are plotted in figure 9, along with the results of Camfield & Street (1969), Chan & Street (1971), Byatt-Smith (1971), Oikawa & Yajima (1973), Maxworthy (1976), and (17a, b) for $A = B$. We have excellent agreement for amplitudes up to 0·30.

To test the existence of the wave train for small amplitudes we have reconsidered the case with amplitude 0·1, with $\Delta x = \Delta t = 0{\cdot}01$, in different stages. Because for small amplitudes the solitary wave has a large extension, the x and t variables were redimensionalized by the wavenumber. This introduced minor changes in the finite-difference equations and boundary conditions where derivatives were involved. We started with a grid of 2000 points till the maximum run-up occurred. Then the grid was enlarged to 3000 points, and later to 4000 points. We carried the integration till the time step 3740. The surface elevation of the last time step is plotted in comparison with the initial profile in figure 10. The discrepancies in the conservation laws of mass, energy, Bernoulli and momentum are no more than 2×10^{-8}, $3{\cdot}6 \times 10^{-8}$, $1{\cdot}3 \times 10^{-5}$ and $1{\cdot}3 \times 10^{-5}$ respectively, for all of the time of integration. As is evident from figure 10, the wave train has not completely separated from the main wave. The amplitude of the reflected wave up to the time step 3446 reached 99·8 % of its initial value. The energy deficit calculated from (27) is 0·1 % of the original value. As in the case that

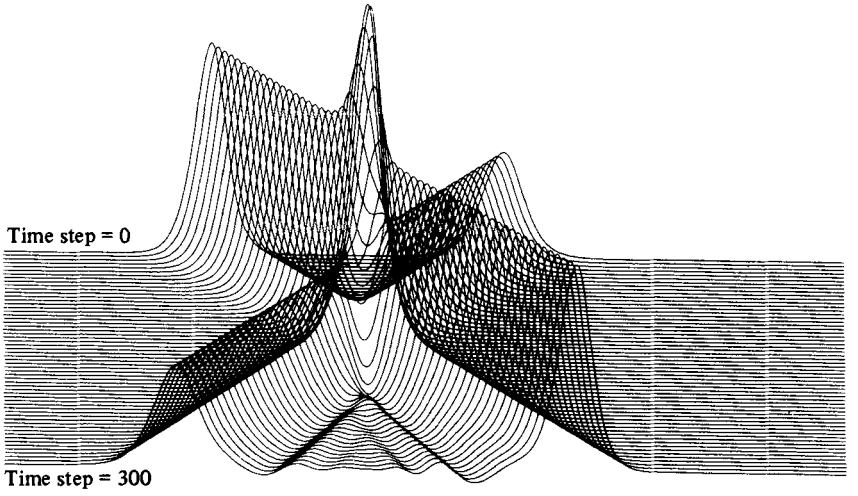

FIGURE 11. Weak interaction of 0·5 and 0·25 amplitude solitary waves. Elevation versus x and t.

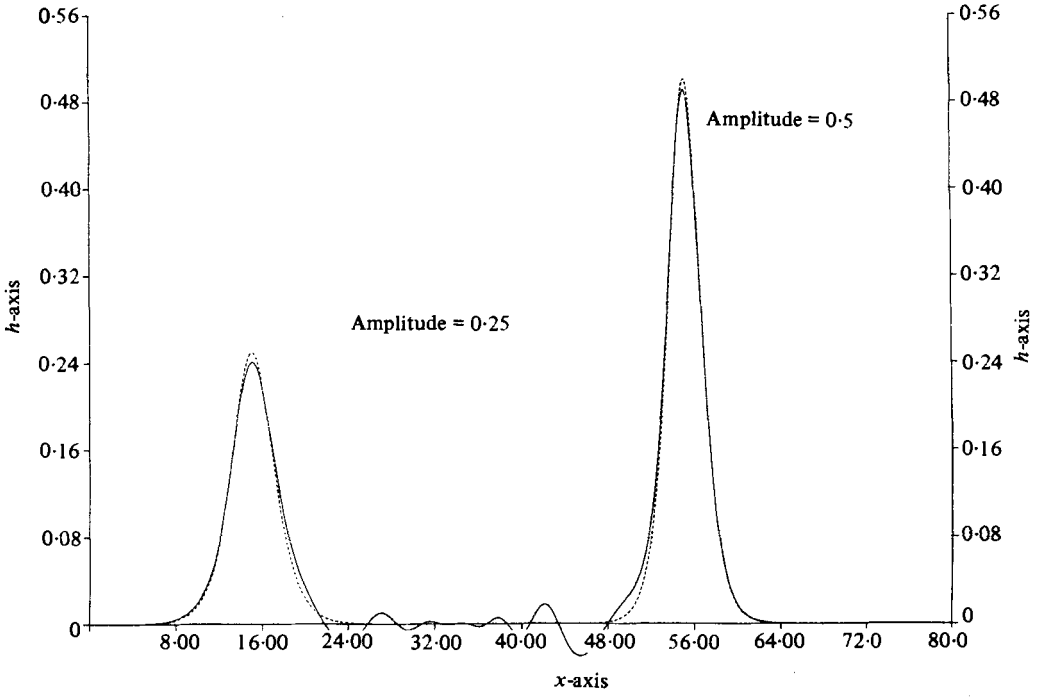

FIGURE 12. Comparison with initial profile of the last profile in figure 11 versus x. Actual time = 29·9.

we discussed earlier (for collision of two waves with amplitude 0·5), this deficit is much bigger than the error in the constancy of the energy of our numerical calculation. In both cases, we are certain that the wavelets, at least those in the leading part of the wave train, are not numerical noise. We also note that the difference in amplitude between the reflected and the original wave is much less than the cube of the original

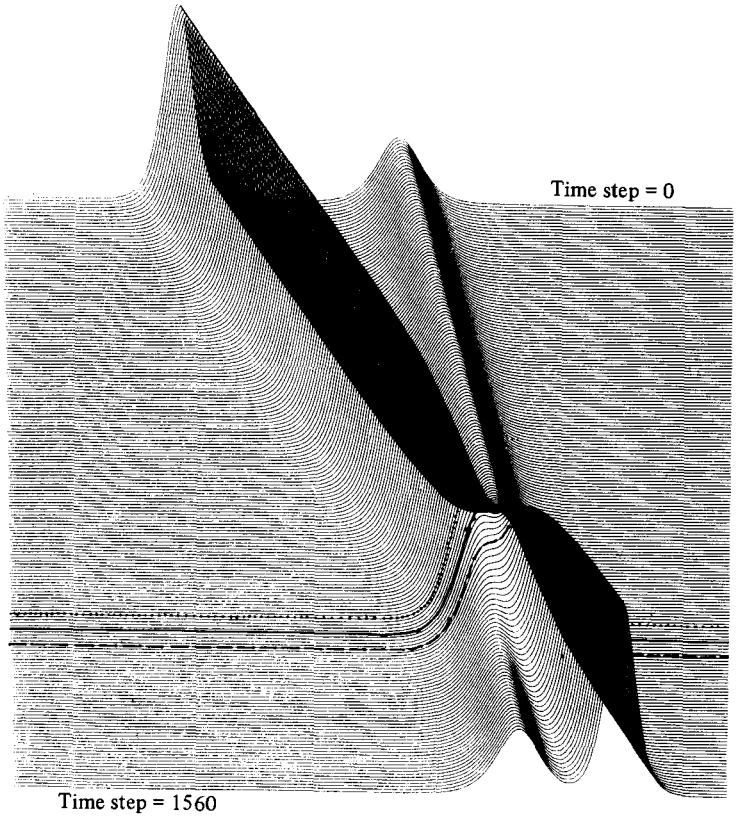

FIGURE 13. Strong interaction of 0·6 and 0·2 amplitude solitary waves. Elevation versus $\xi\ (= x-t)$, t time steps 9–1541.

amplitude, a discrepancy which is beyond the third order of approximation in the perturbation calculation presented in paper 1. Our results indicate that the recovery of a solitary wave in a head-on collision is not 100 %. The discrepancy is amplitude-dependent: 99·8 % for waves of amplitude of 0·1 and 98 % for waves of amplitude of 0·5.

(ii) *Wave–wave weak interaction*

We consider the collision of two solitary waves with different amplitudes. The initial condition is given by a linear sum of two well-separated solitary waves of amplitudes 0·5 and 0·25. The waves were set on a head-on collision course. We used exponential-decay boundary conditions on both ends of the range of integration. The grid size was $\Delta x = 0{\cdot}1, \Delta t = 0{\cdot}1$ and the range consisted of 2000 grid points. We integrated up to 300 time steps. Details of the profile are given in figure 11. The maximum amplitude of the wave trains trailing behind each solitary wave depend on the amplitudes of the solitary waves. In figure 12 we compare the numerical result after the collision with the linear sum of exact solitary waves, and notice a slight discrepancy in amplitude. The maximum run-up calculated is (0·8199) while (17a) gives (0·8359). Considering that the next-order term in (17a) is of order of magnitude $A^2B^2 = 0{\cdot}0156$, the accuracy we have is excellent.

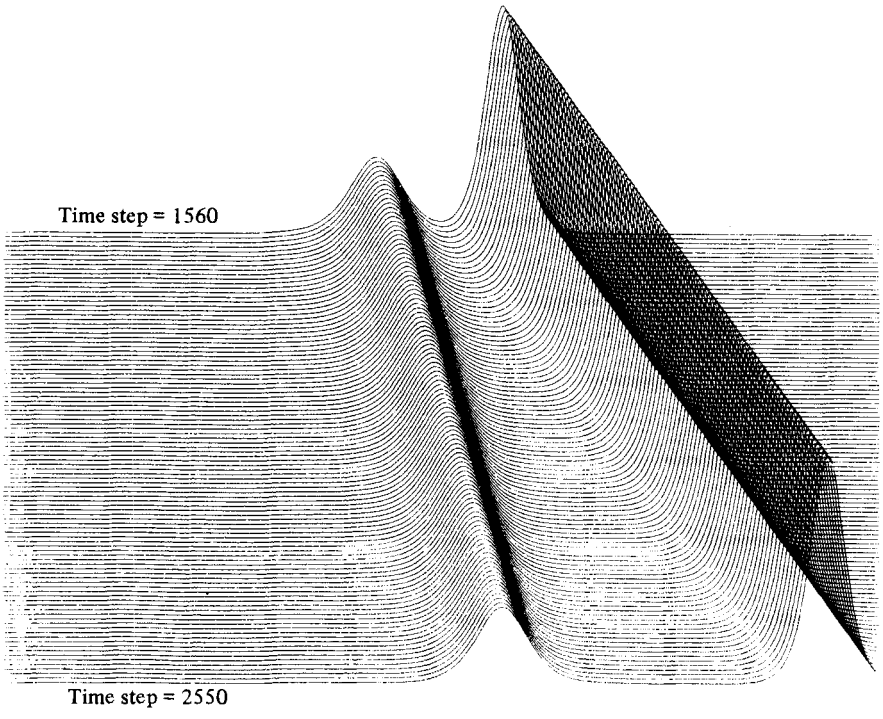

FIGURE 14. Same as figure 13. Time steps 1560–2550.

(iii) *Wave–wave strong interaction*

We consider the overtaking collision of two solitary waves of amplitudes 0·6, 0·2. The initial conditions are given by a linear sum of two well-separated solitary waves. The waves are set to move in one direction in a moving grid of unit speed consisting of 800 points with $\Delta x = \Delta t = 0{\cdot}1$. In this moving grid the integration is carried till the time step 1550. In figure 13 we plot the surface elevation versus x and t from $t = 0$ up to this time step. We accentuated the wave profiles at three different instants of time to elucidate the time evolution of the interaction. As the big wave is overtaking the smaller one, the latter increases and the former decreases in amplitude until the two become equal. This state is shown by the middle profile (solid line), which is nearly symmetric with a minimum centred between two equal maxima. However, before this happened, the maximum height of the small wave disappeared once under the big wave, as evidenced from the dotted profile. The disappearance of the peak of the small wave recurred once again after the big wave re-emerged (now on the right side of the small wave) from the state of symmetry. This is indicated by the dashes.

The time history of the collision described above fits in with case (*b*) of a theory expounded by Lax (1968) using the K–dV equation. The speed ratio in the present case is 3, which puts our case between cases (*b*) and (*c*) of Lax.†

The grid was enlarged from 800 to 1100 points after time step 1150. Figure 14 shows the profiles up to time step 2250. From figures 13 and 14, it is easily seen that the big wave is shifted forward while the small wave is shifted backward owing to collision. The numerical values for these shifts are: big wave 2·3, small wave 3·6.

† This behaviour was observed experimentally by Weidman & Maxworthy (1978).

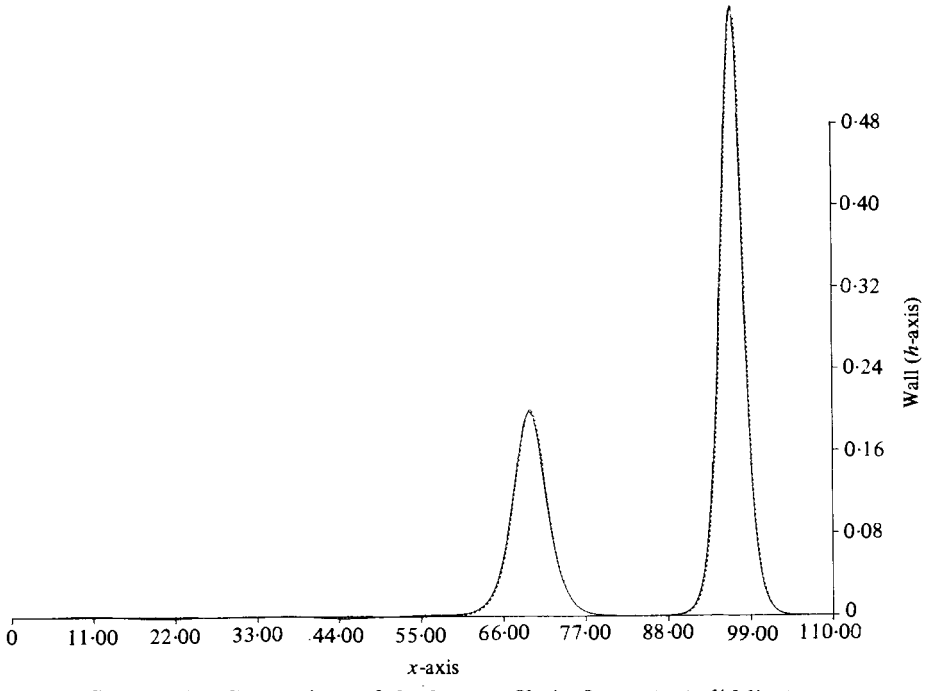

FIGURE 15. Comparison of the last profile in figure 14 (solid line) and the initial data (dotted line).

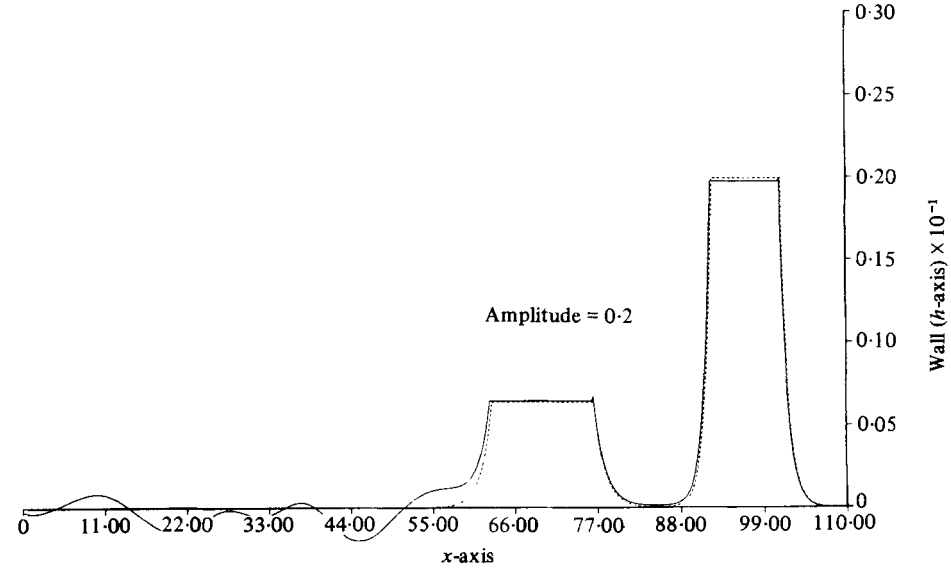

FIGURE 16. Enlargement of figure 15. Actual time = 255·60.

The corresponding theoretical values based on the K–dV equation are 1·96 and 3·4, as given by Hirota (1971), Gardner *et al.* (1974) and Whitham (1974). The small discrepancies are probably due to some higher-order effects contained in the equation that we used.

In figure 15 we compare the wave profile at time step 2250 with the initial solitary

waves. The amplitudes of both waves have recovered 99 % of their initial values. However, the wavy structure trailing behind the smaller wave after collision, as amplified in figure 16, is of much smaller amplitude than that in a head-on collision (compare figures 16 and 12). The amplitude of the oscillations in figure 16 is of the same size as the error in the constants of motion. The somewhat irregular oscillations in this case could very well be due to the numerical error. Further investigation with finer grids is needed to ascertain the existence of a wave train in the case of overtaking collisions.

This research has been sponsored by the National Science Foundation, CME-801-2192 Fluid Mechanics Program, and by the Office of Naval Research, U.S. Navy. One of the authors (R. Mirie) wishes to express his appreciation for all the help and support of H.R.H. Prince Salman Ben Abdul Aziz Al Saud.

REFERENCES

ABDULLEOV, KH. O., BOGOLUBSKY, I. L. & MAKHANKOV, V. G. 1976 One more example of inelastic soliton interaction. *Phys. Lett.* **56**A, 427–428.

BONA, J. L., PRITCHARD, W. G. & SCOTT, L. R. 1980 Solitary-wave interaction. *Phys. Fluids* **23**, 438–441.

BONDESON, A., LISAK, M. & ANDERSON, D. 1979 Soliton perturbations: a variational principle for soliton parameters. *Phys. Scripta* **20**, 479–492.

BYATT-SMITH, J. G. B. 1971 An integral equation for unsteady surface waves and a comment on the Boussinesq equations. *J. Fluid Mech.* **49**, 625–633.

CAMFIELD, F. E. & STREET, R. L. 1969 Shoaling of solitary waves of small amplitude. *A.S.C.E. J., Waterways & Harbours Div.* **95**, 1–22.

CHAN, R. K. C. & STREET, R. L. 1971 A computer study of finite amplitude water waves. *J. Comp. Phys.* **6**, 68–94.

FERNANDEZ, J. C., REINISCH, G., BONDESON, A. & WEILAND, J. 1978 Collapse of a K–dV solution into a weak noise shelf. *Phys. Lett.* **66**A, 175–178.

GARDNER, C. S., GREEN, J. M., KRUSKAL, M. D. & MIURA, R. M. 1974 Korteweg–de Vries equations and generalization. VI. Method for exact solution. *Comm. Pure Appl. Math.* **27**, 97–133.

HIROTA, R. 1971 Exact solution of the Korteweg–de Vries equation for multiple collisions of solitons. *Phys. Rev. Lett.* **27**, 1192–1194.

KARPMAN, V. I. 1979 Soliton evolution in the presence of perturbation. *Phys. Scripta* **20**, 462–478.

LAX, P. D. 1968 Integrals of nonlinear equations of evolution and solitary waves. *Comm. Pure Appl. Math.* **21**, 467–490.

MAXWORTHY, T. 1976 Experiments on collisions between solitary waves. *J. Fluid Mech.* **76**, 177–185.

MIRIE, R. M. 1980 Collisions of solitary waves. Ph.D. thesis, Brown University.

OIKAWA, M. & YAJIMA, N. 1973 Interaction of solitary waves – a perturbation to nonlinear systems. *J. Phys. Soc. Japan* **34**, 1093–1099.

PEREGRINE, D. H. 1966 Calculations of the development of an undular bore. *J. Fluid Mech.* **25**, 321–330.

SU, C. H. & GARDNER, C. S. 1969 Korteweg–de Vries equation and generalizations. III. Derivation of the Korteweg–de Vries equation and Burgers equation. *J. Math. Phys.* **10**, 536–539.

SU, C. H. & MIRIE, R. M. 1980 On head-on collisions between two solitary waves. *J. Fluid Mech.* **98**, 509–525.

WHITHAM, G. B. 1974 *Linear and Nonlinear Waves.* Wiley Interscience.

WEIDMAN, P. & MAXWORTHY, T. 1978 *J. Fluid Mech.* **85**, 417–431.